Noncovalent Interactions

DOI: 10.1002/ange.201405349

Understanding a Host–Guest Model System through ^{129}Xe NMR Spectroscopic Experiments and Theoretical Studies**

Emmanuelle Dubost, Jean-Pierre Dognon, Bernard Rousseau, Gaëlle Milanole, Christophe Dugave, Yves Boulard, Estelle Léonce, Céline Boutin, and Patrick Berthault**

Abstract: *Gaining an understanding of the nature of host–guest interactions in supramolecular complexes involving heavy atoms is a difficult task. Described herein is a robust simulation method applied to complexes between xenon and members of a cryptophane family. The calculated chemical shift of xenon caged in a H_2O_2 probe, as modeled by quantum chemistry with complementary-orbital, topological, and energy-decomposition analyses, is in excellent agreement with that observed in hyperpolarized ^{129}Xe NMR spectra. This approach can be extended to other van der Waals complexes involving heavy atoms.*

Among the hyperpolarized species widely used as NMR spectroscopic probes today, xenon has a specific place, as it combines the very high sensitivity afforded by the optical-pumping step with considerable responsiveness to the local environment; these features translate into an important variation of the NMR spectroscopic parameters. This last decade has seen growing interest in the targeting of biological receptors by the encapsulation of xenon in functionalized host systems (see Refs. [1–5] and references therein). In this biosensing approach based on ^{129}Xe NMR spectroscopy, encapsulated xenon has to exhibit a resonance frequency that is markedly different from the frequency of free xenon. Good candidates for such xenon biosensing are cryptophanes: cage molecules that exhibit high xenon affinity and in which encapsulated xenon takes a specific spectral signature.[6] Even more recently, the concept of smart xenon biosensors has been proposed, according to which the chemical shift of caged xenon varies when the host system is in the presence of the targeted receptor or analyte.[7,8] A detailed understanding and reliable modeling of the interactions responsible for such effects on the resonance frequency of caged xenon are therefore of high value. In this study, weak interactions (qualified as "difficult to elucidate" by Taratula et al.)[9] were clearly identified, visualized, and quantified by using quantum chemistry with energetic and topological analyses.

For this proof of concept, we chose a reaction that enables the chemical transformation of the cryptophane structure by a small reactant. Ideally, this reaction has to strongly modify the electronic properties of the xenon host. The chemical reaction of an arylboronic acid group with hydrogen peroxide to give a phenol satisfies the abovementioned criteria. Indeed, the boronic acid function is an electron-withdrawing group, whereas the phenol group is an electron-donating group. The cryptophane-111 structure was chosen, as 1) it displays the highest affinity for xenon both in organic solvents[10] and water,[11] 2) tiny chemical modifications on the aromatic rings are expected to strongly influence the chemical shift of caged xenon, and 3) since it is the smallest cryptophane representative, although far from simple, theoretical calculations should be more straightforward. Moreover, several boronic functionalities can be grafted on a cryptophane-111 core to form, after oxidation, different molecular cages. Water-soluble cryptophane-111 hexaboronic acid (compound **0**, Scheme 1) was thus synthesized by using the bromination step previously described.[12] Treatment of the hexabrominated compound with *n*BuLi, followed by the addition of 2-isopropoxy-4,4,5,5-tetramethyl-1,3,2-dioxaborolane, furnished the expected hexaboronic cryptophane.

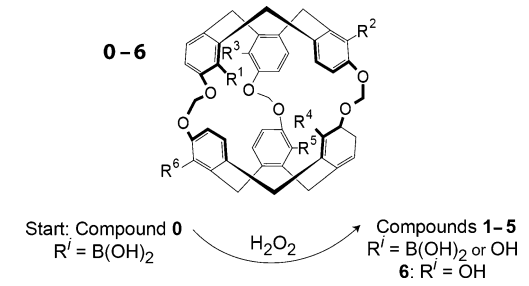

Scheme 1. Transformation of arylboronic groups into phenol groups by H_2O_2 in the cryptophane-111 structure.

The one-scan hyperpolarized ^{129}Xe NMR spectrum of a 0.97 mM aqueous solution of **0** displays a single signal in the

[*] E. Dubost, B. Rousseau, G. Milanole, C. Dugave
iBiTec-S/SCBM, LabEx LERMIT, CEA Saclay
91191 Gif-sur-Yvette (France)
J.-P. Dognon
Laboratoire de Chimie Moléculaire et Catalyse pour l'Energie
IRAMIS/NIMBE, URA 3299 CEA/CNRS, CEA Saclay
91191 Gif-sur-Yvette (France)
E-mail: jean-pierre.dognon@cea.fr
Y. Boulard, E. Léonce, C. Boutin, P. Berthault
Laboratoire Structure et Dynamique par Résonance Magnétique
IRAMIS/NIMBE, URA 3299 CEA/CNRS, CEA Saclay
91191 Gif-sur-Yvette (France)
E-mail: patrick.berthault@cea.fr

[**] For this research, access to the HPC resources of [CCRT/CINES/IDRIS] was granted under the allocation x2014086146 made by GENCI (Grand Equipement National de Calcul Intensif). Support from the French Ministry of Research (project ANR-12-BSV5-0003) and from the Fondation pour la Recherche Médicale (project DCM20111223065) is acknowledged.

Supporting information for this article, including details of the synthesis of compound **0**, details of the NMR spectroscopic experiments, and computational details, is available on the WWW under http://dx.doi.org/10.1002/anie.201405349.

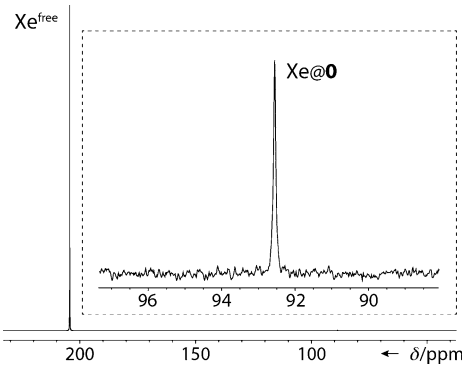

Figure 1. One-scan ^{129}Xe NMR spectrum of a 0.97 mM solution of **0** in D_2O/[D_6]DMSO (11:1 *v*/*v*). In the dashed frame, a zoom of the high-field region of the spectrum is shown, with the caged-xenon resonance.

high-field region (92.5 ppm), thus confirming the high purity of the sample (Figure 1). By recording hyperpolarized ^{129}Xe NMR spectra at different times after solubilization, we verified that the compound did not degrade over the period of a month.

One microliter of H_2O_2 at a concentration of 30% was then added to the cryptophane solution, and ^{129}Xe NMR spectra were recorded at different time periods. Figure 2 displays the high-field region of five such spectra. The first spectrum, recorded 31 min after the addition of hydrogen peroxide, reveals the signal of xenon caged in **0**, along with a second signal at 83.3 ppm, thus separated from the first signal by 9.2 ppm. In a spectrum recorded 3 h after the addition of hydrogen peroxide, the xenon signal at 92.5 ppm has disappeared, whereas several other signals appear at higher field. These new signals are concentrated in two spectral regions, around 73 and 63 ppm. The third displayed spectrum, which was recorded 7 h after the addition of H_2O_2, exhibits new signals at higher field (centered around 53 ppm), whereas the signal at 83.3 ppm has diminished. In the next spectrum, recorded the next day (see the precise times in Figure 2), the group of signals at 73 ppm has disappeared, and a signal appears at 41.9 ppm. Finally, in the last spectrum recorded the following week, the group of signals at 63 ppm has disappeared, and a new signal appears at 30.7 ppm.

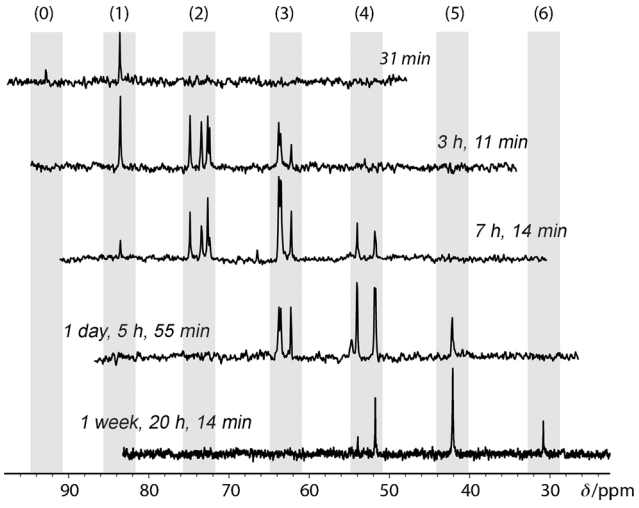

Figure 2. Some of the one-scan ^{129}Xe NMR spectra recorded after the addition of H_2O_2 (high-field region).

From these observations, it is clear that H_2O_2 reacts with the boronate groups of the cryptophane (Scheme 1). All told, six new groups of signals appear, with pairwise spectral separation between 9 and 10 ppm. It seems clear that these seven groups of signals correspond to xenon caged in cryptophanes with different degrees of transformation of the boronate groups into hydroxy groups (the number in parentheses in Figure 2 indicates the number of hydroxy functionalities on the cryptophane). This hypothesis is substantiated by both HPLC–MS and a thorough observation of the ^{129}Xe NMR spectra (see the Supporting Information). HPLC–MS clearly shows the six groups of compounds with the correct masses. In the ^{129}Xe NMR spectra, xenon in the native cryptophane **0**, in the monohydroxylated cryptophane **1**, in the pentahydroxylated cryptophane **5**, and in the final product, the hexahydroxylated cryptophane **6**, gives rise to single resonances. Conversely, multiple resonances in each spectral cluster appear for xenon in the doubly, triply, and fourfold hydroxylated cryptophanes (situations **2**, **3**, and **4**), as expected, as several regioisomers of these cryptophanes can be present. These results substantiate the major role of the nature of the chemical groups carried by the aromatic rings on the chemical shift of caged xenon; in any case, it is larger than the influence of their relative position.

Several simulations of host–guest complexes, including those of cryptophanes,[13–15] C_{60},[16–18] and clathrates,[19,20] have been performed by quantum chemistry or molecular dynamics. None of them elucidated the nature of the host–guest interaction or the origin of the xenon chemical shift. The combined use of joint- and complementary-orbital, topological, and energy-decomposition (EDA) analyses is a powerful approach to gain an understanding of the host–guest interaction[21] that leads to these chemical shift values. Traditional density functionals do not include dispersion and are not appropriate for the description of the xenon–cage interaction. They must at least be augmented by a dispersion-energy correction, for example, by the Grimme DFT-D method;[22,23] however, to recover most of the interaction, explicitly correlated methods are required. We explored the xenon–cage interaction on the basis of the second-order Møller–Plesset perturbation theory (MP2), which natively includes dispersion effects and is a good compromise between efficiency and accuracy. A pair-interaction energy-decomposition analysis (PIEDA)[24] was performed at the FMO-MP2 level of theory[25] (see the Supporting Information for details). We found that the xenon–cage binding energy (ΔE_{int}) is a negative value in the range between −9.4 and −12.4 kcal mol^{-1} (see Table 1). EDA indicated that the encapsulated xenon atom is stabilized mainly by attractive dispersion forces.

The substitution of $B(OH)_2$ groups in **0** by OH groups to give compounds **1**–**6** led to structures with similar optimized geometries. The geometry differences arise mainly from pseudoaxial (OH) versus pseudoequatorial $B(OH)_2$ substituent orientations, which give rise to a slightly more compact structure for compound **0** (see Figure S8a,b in the Supporting

Table 1: Analysis of bonding in the Xe@***n*** series (n = **0**–**6**) and ^{129}Xe NMR chemical shifts (theoretical δ_{scal} and experimental δ_{exp} values in ppm).[a]

n	ΔE_{int}	ΔE_{EX}	ΔE_{ES}	ΔE_{CT}	ΔE_{DI}	δ_{scal}	δ_{exp}
0	−12.4	22.3	−8.4	−4.9	−21.3	91.3	92.5
1	−10.7	22.2	−8.3	−4.5	−20.2	86.4	83.3
2	−10.4	21.8	−8.2	−4.3	−19.7	71.5	73.1
3	−10.2	21.2	−8.0	−4.1	−19.4	61.8	62.9
4	−10.1	20.7	−7.8	−3.9	−19.1	52.3	52.6
5	−9.7	20.3	−7.6	−3.7	−18.6	43.5	41.9
6	−9.4	18.8	−7.1	−3.3	−17.8	30.1	30.7

[a] Components of the interaction energy (E_{int}): electrostatic (ES), exchange-repulsion (EX), charge transfer (CT), and dispersion (DI). All values in kcal mol^{-1}. For the δ_{exp} value of compounds **2**–**4**, the average chemical shift is given.

Information). As a result, small changes in the interaction energy and its components are calculated, with higher stabilizing terms for Xe@**0**. For all compounds, the dispersion term contributes approximately 60% to the total attractive interactions, the electrostatic term to approximately 25%. These two terms govern the host–guest interactions. This result is compatible with the finding of Haberhauer et al.,[26] who showed the important role of attractive dispersion energy in $CHCl_3$–cryptophane complexes. Johnson and co-workers[27] recently introduced a method for studying noncovalent interactions (NCIs) on the basis of the electron density (ρ), the reduced gradient of the density ($s = |\nabla\rho|/(2(3\pi^2)^{1/3}\rho^{4/3})$), and the Laplacian of the density ($\nabla^2\rho$). The approach enables the identification of the interactions in real space, and thus the graphical visualization of the regions in which noncovalent interactions occur. Figure 3 shows the dispersion-interaction regions in the Xe@**0** and Xe@**6** complexes as green spatial zones computed at the MP2 level (see the Supporting Information for details). These large spatial-interaction zones are in full agreement with the energy-decomposition analyses, according to which the noncovalent interactions control the stabilization of the complex. Among these noncovalent interactions, the phenyl-ring–xenon interaction is predominant, and the adaptability of the cryptophane optimizes these interactions. This major effect regulates the encapsulation of xenon.

Because the difference in the geometries and in the nature of the xenon–cage interaction in compounds **0**–**6** is small, the interpretation of the large changes in the xenon chemical shift along the series is not straightforward. The ^{129}Xe isotropic shielding was calculated on the basis of the DFT/GIAO shielding tensor, the components of which are formally defined by the equation:[28,29]

$$\sigma_{\alpha\beta} = \frac{\partial^2 E}{\partial\mu_\alpha \partial B_\beta}$$

in which E is the total electronic energy of the molecule, B is the external magnetic field, and μ is the magnetic moment of the nucleus of interest. The calculated chemical shift was obtained from σ and then scaled with a linear equation (see the Supporting Information for details). These scaled chemical shifts (δ_{scal}) are in very good agreement with the

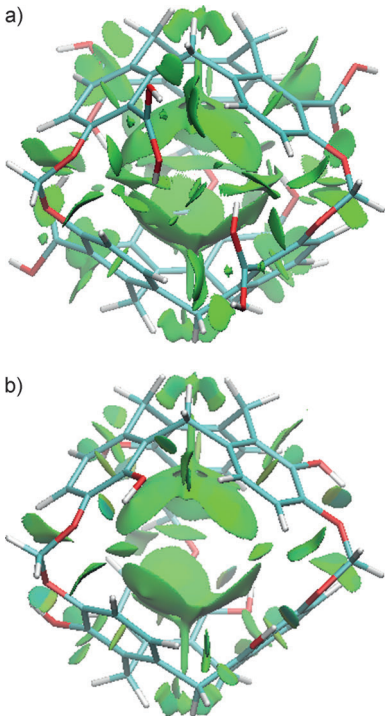

Figure 3. Structure of the complexes of xenon with a) cryptophane **0** and b) cryptophane **6**. The noncovalent-interaction regions appear in green (the central xenon atom was removed for clarity).

experimental values (δ_{exp}; Table 1), with a coefficient of determination $R^2 = 0.994$.

To obtain more insight into the origin of the ^{129}Xe chemical shift, we further decomposed the theoretical magnetic shielding tensors σ into paramagnetic (σ_p) and diamagnetic (σ_d) components (the two terms are present in a ZORA scalar relativistic calculation). Whereas the diamagnetic contribution is nearly constant along the series, the variation in the ^{129}Xe nuclear magnetic shielding originates from the paramagnetic contribution (see Table S1 in the Supporting Information). This evolution may be associated with a change in the electron-donating/withdrawing character of carbon substituents in **0**–**6**, which was analyzed with multipole derived charges (MDC) calculations.[30] MDC analysis performs better than other methods (e.g. the Mulliken method) for analysis of the substituent effects on the charge distribution.[30] The carbon atom has a negative charge (−0.38) when attached to a $B(OH)_2$ group (in compound **0**) and a positive charge (+0.37) when attached to an OH group (in compound **6**). Calculations indicate a low charge delocalization on the phenyl ring (see Figure S9 a,b). Summing of the MDCs of the carbon atoms that carry the substituent groups along the series resulted in a total charge variation of −2.27 (for **0**) to +2.21 (for **6**) with a clear correlation ($R^2 = 0.9994$) with the experimental chemical shifts (see Figure S10). This effect, amplified by a non-negligible mixing of the 5p orbitals of Xe with the cryptophane phenyl-ring orbitals (ca. 15% from a symmetrized fragment orbital analysis) contributes to a large anisotropy of the quadrupole-moment tensor (Figure 4). The changes in the electron distribution of the phenyl ring along the series induce a change in the electric-

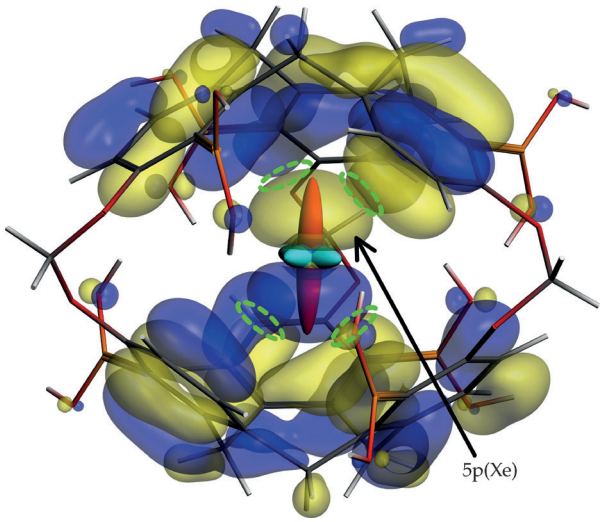

Figure 4. Interaction of the 5p(Xe) orbital with the phenyl-ring orbitals of cryptophane **0**. Examples of interaction regions are highlighted by dashed green ellipses. The quadrupole-tensor components are also represented.

field gradient (EFG) at the xenon nucleus, as shown by the evolution of the largest component of the diagonalized EFG tensor V_{zz} (see the Supporting Information for details). This change in the EFG is clearly the origin of the observed evolution of the ^{129}Xe chemical shift from **0** to **6**.

This molecular system and approach constitute a precious and unique model for validating an ensemble of theoretical tools. They enable a thorough understanding of host–guest interactions, as well as their influence on the NMR spectroscopic parameters. For the first time, all the components of the interaction were identified, and the origin of the ^{129}Xe chemical shift value of caged xenon determined. We have shown that, even for the current case, in which an electron-withdrawing group is replaced with an electron-donating group, the electrostatic forces are not the predominant factor for the stabilization of the complex. Rather, primarily dispersion forces account for the stabilization of the complex. The ^{129}Xe chemical shift originates from the electronic effect of the substituent group.

It is the first time that such precision has been possible for the prediction of xenon chemical shifts; the chemical shift variation between two consecutive members of the family is approximately 4% of that between xenon caged in a cryptophane and free xenon in water. Such a model will be of high interest for the prediction of the effects of other cryptophane substituents on the chemical shift of caged xenon, and particularly helpful in our research dealing with "smart" xenon biosensors.[7,8] In future studies, we will also seek to understand the kinetic parameters of the interaction, with a particular emphasis on the solvent effect, to design very potent xenon–host systems optimized for HyperCEST detection.[31]

Received: May 16, 2014
Published online: July 22, 2014

Keywords: cryptophanes · host–guest systems · NMR spectroscopy · quantum chemistry · xenon

[1] M. M. Spence, E. J. Ruiz, S. M. Rubin, T. J. Lowery, N. Winssinger, P. G. Schultz, D. E. Wemmer, A. Pines, *J. Am. Chem. Soc.* **2004**, *126*, 15287 – 15294.
[2] P. Berthault, G. Huber, H. Desvaux, *Prog. Nucl. Magn. Reson. Spectrosc.* **2009**, *55*, 35 – 60.
[3] O. Taratula, Y. Bai, E. L. D'Antonio, I. J. Dmochowski, *Supramol. Chem.* **2014**, 1 – 8.
[4] K. K. Palaniappan, R. M. Ramirez, V. S. Bajaj, D. E. Wemmer, A. Pines, M. B. Francis, *Angew. Chem.* **2013**, *125*, 4949 – 4953; *Angew. Chem. Int. Ed.* **2013**, *52*, 4849 – 4853.
[5] S. Klippel, J. Döpfert, J. Jayapaul, M. Kunth, F. Rossella, M. Schnurr, C. Witte, C. Freund, L. Schröder, *Angew. Chem.* **2014**, *126*, 503 – 506; *Angew. Chem. Int. Ed.* **2014**, *53*, 493 – 496.
[6] T. Brotin, J. P. Dutasta, *Chem. Rev.* **2009**, *109*, 88 – 130.
[7] N. Kotera, N. Tassali, E. Léonce, C. Boutin, P. Berthault, T. Brotin, J.-P. Dutasta, L. Delacour, T. Traoré, D.-A. Buisson, F. Taran, S. Coudert, B. Rousseau, *Angew. Chem.* **2012**, *124*, 4176 – 4179; *Angew. Chem. Int. Ed.* **2012**, *51*, 4100 – 4103.
[8] N. Tassali, N. Kotera, C. Boutin, E. Léonce, Y. Boulard, B. Rousseau, E. Dubost, F. Taran, T. Brotin, J.-P. Dutasta, P. Berthault, *Anal. Chem.* **2014**, *86*, 1783 – 1788.
[9] O. Taratula, P. A. Hill, N. S. Khan, P. J. Carroll, I. J. Dmochowski, *Nat. Commun.* **2010**, *1*, 148.
[10] H. A. Fogarty, P. Berthault, T. Brotin, G. Huber, H. Desvaux, J. P. Dutasta, *J. Am. Chem. Soc.* **2007**, *129*, 10332 – 10333.
[11] R. M. Fairchild, A. I. Joseph, K. T. Holman, H. A. Fogarty, T. Brotin, J. P. Dutasta, C. Boutin, G. Huber, P. Berthault, *J. Am. Chem. Soc.* **2010**, *132*, 15505 – 15507.
[12] E. Dubost, N. Kotera, S. Garcia-Argote, Y. Boulard, E. Léonce, C. Boutin, P. Berthault, C. Dugave, B. Rousseau, *Org. Lett.* **2013**, *15*, 2866 – 2868.
[13] D. N. Sears, C. J. Jameson, *J. Chem. Phys.* **2003**, *119*, 12231 – 12244.
[14] E. J. Ruiz, D. N. Sears, A. Pines, C. J. Jameson, *J. Am. Chem. Soc.* **2006**, *128*, 16980 – 16988.
[15] A. Bagno, G. Saielli, *Chem. Eur. J.* **2012**, *18*, 7341 – 7345.
[16] D. N. Sears, C. J. Jameson, *J. Chem. Phys.* **2003**, *118*, 9987 – 9989.
[17] J. Autschbach, E. Zurek, *J. Phys. Chem. A* **2003**, *107*, 4967 – 4972.
[18] M. Straka, P. Lantto, J. Vaara, *J. Phys. Chem. A* **2008**, *112*, 2658 – 2668.
[19] S. Alavi, P. Dornan, T. K. Woo, *ChemPhysChem* **2008**, *9*, 911 – 919.
[20] D. Stueber, C. J. Jameson, *J. Chem. Phys.* **2004**, *120*, 1560 – 1571.
[21] J.-P. Dognon, *Coord. Chem. Rev.* **2014**, *266* – 267, 110 – 122.
[22] S. Grimme, *J. Comput. Chem.* **2006**, *27*, 1787 – 1799.
[23] S. Grimme, J. Antony, S. Ehrlich, H. Krieg, *J. Chem. Phys.* **2010**, *132*, 154104.
[24] D. G. Fedorov, K. Kitaura, *J. Comput. Chem.* **2007**, *28*, 222 – 237.
[25] K. Kitaura, E. Ikeo, T. Asada, T. Nakano, M. Uebayasi, *Chem. Phys. Lett.* **1999**, *313*, 701 – 706.
[26] G. Haberhauer, S. Woitschetzki, H. Bandmann, *Nat. Commun.* **2014**, *5*, 3542.
[27] E. R. Johnson, S. Keinan, P. Mori-Sánchez, J. Contreras-García, A. J. Cohen, W. Yang, *J. Am. Chem. Soc.* **2010**, *132*, 6498 – 6506.
[28] G. Schreckenbach, T. Ziegler, *J. Phys. Chem.* **1995**, *99*, 606 – 611.
[29] G. Schreckenbach, T. Ziegler, *Int. J. Quantum Chem.* **1997**, *61*, 899 – 918.
[30] M. Swart, P. T. van Duijnen, J. G. Snijders, *J. Comput. Chem.* **2001**, *22*, 79 – 88.
[31] L. Schröder, T. J. Lowery, C. Hilty, D. E. Wemmer, A. Pines, *Science* **2006**, *314*, 446 – 449.